THE JOURNAL OF BIOLOGICAL CHEMISTRY VOL. 288, NO. 37, pp. 26372–26384, September 13, 2013
© 2013 by The American Society for Biochemistry and Molecular Biology, Inc. Published in the U.S.A.

Structural Model of the Anion Exchanger 1 (SLC4A1) and Identification of Transmembrane Segments Forming the Transport Site[S]

Received for publication, March 5, 2013, and in revised form, July 10, 2013 Published, JBC Papers in Press, July 11, 2013, DOI 10.1074/jbc.M113.465989

Damien Barneaud-Rocca[‡§¶], Catherine Etchebest[‖‡‡§§], and Hélène Guizouarn[‡§¶1]**

*From the [‡]Université Nice Sophia Antipolis, Institut de Biologie Valrose, UMR7277, 06100 Nice, France, [§]CNRS, UMR7277, 06100 Nice, France, [¶]INSERM U1091, 06100 Nice, France, [‖]Dynamique des Structures et des Interactions des Macromolécules Biologiques, INSERM, U665, F-75015 Paris, France, **Université Paris Diderot, Sorbonne Paris Cité, UMR_S665, F-75015 Paris, France, [‡‡]Institut National de la Transfusion Sanguine, F-75015 Paris, France, and [§§]Laboratoire d'Excellence GR-Ex, 6 rue Alexandre Cabanel, 75739 Paris Cedex, France*

Background: There is still no high resolution three-dimensional structure available for the membrane-spanning domain of anion exchanger 1 (AE1).
Results: A three-dimensional model of AE1 membrane-spanning domain has been generated *in silico* and experimentally assessed.
Conclusion: Transmembrane segments forming AE1 transport site have been identified.
Significance: This is the first three-dimensional model of AE1 membrane-spanning domain based on a cation symporter.

The anion exchanger 1 (AE1), a member of bicarbonate transporter family SLC4, mediates an electroneutral chloride/bicarbonate exchange in physiological conditions. However, some point mutations in AE1 membrane-spanning domain convert the electroneutral anion exchanger into a Na^+ and K^+ conductance or induce a cation leak in a still functional anion exchanger. The molecular determinants that govern ion movement through this transporter are still unknown. The present study was intended to identify the ion translocation pathway within AE1. In the absence of a resolutive three-dimensional structure of AE1 membrane-spanning domain, *in silico* modeling combined with site-directed mutagenesis experiments was done. A structural model of AE1 membrane-spanning domain is proposed, and this model is based on the structure of a uracil-proton symporter. This model was used to design cysteine-scanning mutagenesis on transmembrane (TM) segments 3 and 5. By measuring AE1 anion exchange activity or cation leak, it is proposed that there is a unique transport site comprising TM3–5 and TM8 that should function as an anion exchanger and a cation leak.

The anion exchanger 1 (AE1,[2] SLC4A1, or band 3) is the main membrane protein in vertebrate red cells. It fulfills different tasks in these cells: a structural role by linking plasma membrane to cytoskeleton, a respiratory role by improving CO_2 transport capacity of red cells, and an antigenic function (Diego blood group and senescence), and it is also involved in cytokinesis and red cell volume regulation (1). At the molecular level, this protein is divided into two main structural domains: a cytoplasmic N-terminal domain (about 400 amino acids) and a membrane-spanning domain (about 450 amino acids) with a short C-terminal tail in the cytoplasm. These two entities seem to function independently: the large cytoplasmic domain is involved in interactions with enzymes, hemoglobin, and structural proteins, whereas the membrane-spanning domain is responsible for the transport activity of the protein (2, 3). In addition to red cells, AE1 is also expressed in kidney α-intercalated cells and cardiac myocytes (4). In physiological conditions, AE1 exchanges one chloride for one bicarbonate by an electroneutral transport mechanism with the driving force for ion movement provided by their electrochemical gradient. A few years ago, some specific point mutations were characterized and proposed to convert the electroneutral anion exchanger into a cation-conductive pathway (5, 6). These mutations are associated with human pathologies (hereditary hemolytic anemia and distal renal tubular acidosis) (7–10). In addition to naturally occurring mutations identified in patients with hereditary stomatocytosis or distal renal tubular acidosis, a sequence-function analysis of AE1 revealed other amino acids crucial for transport properties of the protein (11). Unexpected transport activity of AE1 had already been suggested in the past: Tanner and co-workers (12) had shown that human AE1 could behave as a conductive pathway when two putative membrane-spanning helices in the membrane domain of the protein were removed. These data supported the work of Motais and co-workers (13–16) who showed that trout AE1 forms an anion conductive pathway permeable to organic (taurine and choline) and inorganic (Na^+ and K^+) ions in response to decreased ionic strength in red cells. Moreover, AE1 is also able to mediate a proton-anion cotransport when protonated (17, 18).

[S] This article contains supplemental Figs. 1–6 and Tables 1 and 2.

[1] To whom correspondence should be addressed: Inst. de Biologie de Valrose, Bâtiment de Sciences Naturelles, 28 av. Valrose, 06108 Nice Cedex 2, France. E-mail: helene.guizouarn@unice.fr.

[2] The abbreviations used are: AE, anion exchanger; TM, transmembrane; hAE1, human AE1; MBS, modified Barth's saline; PCMBS, *para*-chloromercuribenzene sulfonate; MTSEA, 2-aminoethyl methanethiosulfonate hydrobromide; MTSET, 2-(trimethylammonium)ethyl methanethiosulfonate bromide; MTSES, 2-sulfonatoethyl methanethiosulfonate; DIDS, 4,4′-diisothiocyanostilbene-2,2′-disulfonate; NI, non-injected; g d.w., g of dry weight.

Thus, transport features of AE1 seem to be flexible in response to different stimuli such as mutations (point mutations or deletions), intracellular ionic strength, and pH. The identification of AE1 as a key actor in some types of hereditary stomatocytosis associated with cation-leaky red cells reinforces the interest in understanding the transport process through AE1 protein. Although the three-dimensional structure of AE1 cytoplasmic domain has been solved, the three-dimensional structure of the membrane-spanning domain is not yet available with a resolution high enough to determine the helical packing of the entire membrane domain or to provide insights into the transport mechanism at the molecular level. Thus, our present understanding of ion transport is mainly based on biochemical and functional studies. In an attempt to define the AE1 transport site, cysteine-scanning mutagenesis has been used, and it was shown that the eighth putative helix (TM8) in AE1 membrane-spanning domain lined the anion exchange site (19). Moreover, it has been proposed that this putative TM8 was also involved in the cation leak induced by specific point mutations in AE1 (11). These data point to a unique transport site in the AE1 membrane domain. Its transport mechanism and selectivity could then be modified by specific point mutations.

To further understand the topology and the structure of the AE1 transport site, we combined *in silico* protein modeling and site-directed mutagenesis. A three-dimensional model of AE1 membrane-spanning domain was generated, and its reliability was assessed by experimental and bibliographical data mining.

The present data show that putative TM3, TM5, and TM8 form a central core strongly involved in AE1 transport activity. Cysteine-scanning mutagenesis in these helices allowed identification of residues lining the anion exchange pathway in WT AE1. Moreover, working with a point-mutated AE1 (H734R) in which the anion exchange was converted into a cation leak, it was shown that the same domain was also involved in cation transport. Some key amino acids in TM5 control anion exchange activity of the protein: their substitution abolished anion exchange activity and/or induced a Na^+ and K^+ leak. This study proposes a spatial organization of the membrane-spanning domain and identifies three helices involved in the formation of the transport site. Moreover, this study confirms that this transport site is able to function as an anion exchange and/or a cation leak.

EXPERIMENTAL PROCEDURES

Three-dimensional Structure Prediction and Modeling—The structural modeling of the AE1 human sequence (UniProt accession number P02730) was restricted to the C-terminal sequence, starting from positions 399 to 911. This region encompasses the transmembrane domain. A search for homologous sequences in the Protein Data Bank with BLAST or PSI-BLAST did not retrieve any result except for the cytoplasmic loop (positions 804–835; Protein Data Bank code 1BH7) and the first and second transmembrane spans (positions 399–431 (Protein Data Bank 1BZK) and positions 437–457, respectively) that were solved by NMR. Hence, we resorted to using the I-TASSER method (web service version) that combines a threading approach with fragment prediction. We looked for structural templates with or without imposing constraints. We also tested alternative tools separately such as the HHpred web server, SAM-T08 web server, and DELTA-BLAST tool (Domain Enhanced Lookup Time Accelerated BLAST) recently implemented on the NCBI web site. In the case of I-TASSER, the three first models showed very close C-scores (-2.24, -2.24, and -2.28, respectively) and similar cluster densities. Among the top 10 templates with a significant overlap (>70%) were the glucose symporter (Protein Data Bank code 3DH4) and the uracil transporter (Protein Data Bank code 3QE7). The other prediction tools only retrieved the latter, *i.e.* Protein Data Bank code 3QE7. Despite a rather low identity score (<20%), the E-value and *p* value provided by the HHpred tool encouraged us to proceed with the corresponding template. This template is mainly used in model 3 of I-TASSER.

We then performed a forward-backward approach that consisted of the following: 1) selecting a model in which residues were close enough to be consistent with experimental data available (see "Results" and "Discussion"), 2) designing mutations that could interfere with the putative channel, and 3) refining the model if required. Refinement mainly consisted in rotating TM5 helix around the helical axis to account for proximities deduced from the impact of mutations established by *in vivo* experiments. Local distortions in helical backbone generated by the rotation were removed by imposing helical secondary structure constraints in TM5 and TM8 segments with Modeler software. The model was then relaxed with 1000 steps of steepest descent minimization using the Amber force field implemented in Chimera software (20). In the resulting three-dimensional structure, 92% of the residues are located in favorable or acceptable regions of the Ramachandran diagram. Note that we did not refine conformation of the loops as the presence of the membrane would be required.

Functional Expression of AE1—The experimental procedures are identical to those described in our previous work (11).

Construction of hAE1 cDNA with Point Mutations—The following mutations were constructed: S465C/I/A, L468C, F471C, E472C, E473C, and F475C in putative TM3 and S525C, F526C, I528C, S529C, L530C, F532C, I533C, Y534C, E535C, F537C, K539C, L540C, I541C, and K542C in putative TM5. Site-directed mutagenesis was performed on wild type human erythroid AE1 cloned in pSP65 using the QuikChange site-directed mutagenesis kit (Stratagene) with primers covering 15 bases upstream and downstream of the mutation (Eurogentec, Seraing, Belgium). One positive clone for each mutation was sequenced before further use (Beckman Cogenics, Takeley, UK). The plasmid with H734R point mutation in AE1 was described previously (11). It was used to introduce cysteine in TM5 or TM3, taking advantage of a unique restriction site (PsiI) between TM3 or TM5 and the His^{734} position. The PsiI-HindIII digestion of AE1 plasmids with cysteine in TM3 or TM5 was purified and ligated with the PsiI-HindIII digestion of H734R mutant. Recombinant plasmids carrying the double mutation Cys in TM3 or TM5 and H734R were further sequenced to check constructions.

Oocyte Injection—Isolation and cRNA injection of oocytes were performed as described previously (13). Briefly, HindIII-linearized pSP65hAE1WT and mutant plasmids were tran-

scribed by SP6 RNA polymerase (Ambion transcription kit). Female *Xenopus laevis* were anesthetized with MS222 according to the procedure recommended by our ethics committee.

Stage V-VI oocytes were injected with 10 ng of AE1 (WT and mutated) cRNA. Injected oocytes were maintained at 18 °C in modified Barth's saline (MBS) for 3 or 4 days before running the experiments. MBS composition was as follows: 85 mM NaCl, 1 mM KCl, 2.4 mM $NaHCO_3$, 0.82 mM $MgSO_4$, 0.33 mM $Ca(NO_3)_2$, 0.41 mM $CaCl_2$, 10 mM HEPES, 4.5 mM NaOH, pH 7.4 supplemented with 10 units/ml penicillin and 10 μg/ml streptomycin. For Na^+ and K^+ content measurements, oocytes were incubated in MBS with 0.5 mM ouabain and 5 μM bumetanide. Cl^-/HCO_3^- exchange activity, Na^+ and K^+ contents, Li^+ uptake, and biotin labeling of membrane proteins were determined on the same batch of oocytes 3 or 4 days after injection.

Thiol Alkylations—Thiol alkylation of cysteines was performed by oocyte incubation for 15 min at room temperature in MBS with 1 mM *para*-chloromercuribenzene sulfonate (PCMBS; Sigma) or 5 mM 2-aminoethyl methanethiosulfonate hydrobromide (MTSEA) extemporaneously prepared from stock solutions (1 M in DMSO) stored at −20 °C. For 2-(trimethylammonium)ethyl methanethiosulfonate bromide (MTSET) and 2-sulfonatoethyl methanethiosulfonate (MTSES), they were weighted and solubilized in MBS at 5 mM just before use. (MTS reagents were form Toronto Research Chemicals, Canada). After 15 min, oocytes were washed in MBS and directly assessed for Li^+ uptake experiments or pH_i measurements.

Oocyte Na^+ and K^+ Content Measurements—As published previously (13), oocytes incubated in MBS with ouabain and bumetanide were quickly washed two times in 7.5 ml of Milli-Q water (Millipore) and dried on aluminum foil overnight at 80 °C after removing excess extracellular fluid. Dried oocytes were weighted to determine dry cell solids. Intracellular ions were extracted by suspending dried oocytes in 4 ml of Milli-Q water overnight at 4 °C. Measurements of sodium and potassium were done with a flame spectrophotometer (Eppendorf). For each experiment, a triplicate was made for each condition, and results were expressed as micromoles/gram of dry cell solids.

Cl^-/HCO_3^- Exchange Activity Measurements—Oocyte intracellular pH was measured using selective microelectrodes as published previously (5).

The ability of WT and mutant hAE1 to regulate intracellular pH was assessed by measuring the intracellular pH of oocytes acidified by incubation in medium (63.4 mM NaCl, 1 mM KCl, 24 mM HCO_3^-, 0.82 mM $MgSO_4$, 0.33 mM $Ca(NO_3)_2$, 0.41 mM $CaCl_2$, 5 mM HEPES/NaOH, pH 7.35, 5% CO_2, 95% O_2) and then bathed with MBS without Cl^- (63.4 mM sodium gluconate, 1 mM potassium gluconate, 24 mM HCO_3^-, 0.82 mM $MgSO_4$, 0.74 mM $Ca(NO_3)_2$, 5 mM HEPES/NaOH, pH 7.35, 5% CO_2, 95% O_2). Results are given in ΔpH_i/min ± S.E. ΔpH_i was measured when acidified oocytes were exposed to Cl^--free medium; it corresponds to the initial slope of the alkalinization.

Li^+ Uptake—Li^+ was used as a substitute for Na^+ to measure oocyte cation permeability. To prevent cation movements through the Na,K-ATPase or the Na^+-K^+-2Cl^- cotransporter, Li^+ uptake was done in presence of 5 μM bumetanide and 0.5 mM ouabain in $LiNO_3$ MBS (85 mM $LiNO_3$, 1 mM KNO_3, 2.4 mM $NaHCO_3$, 0.82 mM $MgSO_4$, 0.33 mM $Ca(NO_3)_2$, 0.41 mM $CaCl_2$, 10 mM HEPES, 4.5 mM NaOH, pH 7.4). In each experiment, nine oocytes per condition were incubated for 2 h in $LiNO_3$ MBS at 19 °C. Li^+ was quantified in each individual oocyte by atomic absorption spectrometry with a PerkinElmer Life Sciences AAS3110 instrument. Results are expressed in pmol/oocyte·h (mean ± S.E. of nine oocytes per experimental condition).

AE1 Immunodetection on Oocyte Plasma Membrane—To detect AE1 addressed to the oocyte plasma membrane, surface proteins of oocytes expressing WT or mutated AE1 were labeled with sulfo-NHS-SS-biotin (sulfosuccinimidyl-2-[biotinamido]ethyl-1,3-dithiopropionate; Pierce) in MBS, pH 8 at 4 °C as described previously (11). After a 15-min incubation, the reaction was quenched with buffer (192 mM glycine, 25 mM Tris-HCl, pH 7.5, 0.1 mM $CaCl_2$, 1 mM $MgSO_4$), and oocytes were washed in MBS, pH 8. Oocytes were then lysed mechanically in homogenization buffer (20 mM Tris-HCl, pH 7.4, 250 mM sucrose, 0.5 mM EDTA, 0.5 mM protease inhibitor Pefabloc (Roche Applied Science)), and oocyte membranes were solubilized in radioimmune precipitation assay buffer (150 mM NaCl, 1 mM EDTA, 50 mM Tris-HCl, pH 8, 1% Nonidet P-40, 0.5% deoxycholate, 0.1% SDS, 0.5 mM Pefabloc) for 30 min at 4 °C. Biotin-labeled proteins in the solubilized membranes were isolated by immobilization on avidin resin (Pierce) for 30 min at 4 °C. After washing in radioimmune precipitation assay buffer, biotin-labeled proteins were eluted in SDS-PAGE loading buffer, analyzed by SDS-PAGE, transferred to PVDF membrane (Millipore), and probed with primary antibodies as indicated in the figure legends. Secondary antibodies were anti-rabbit or anti-mouse horseradish peroxidase-coupled (Sigma) and detected by chemiluminescence reaction with Immobilon Western reagent (Millipore) and a Fusion FX7 imaging system (Vilber-Lourmat, France). To compare AE1 expression levels in different samples, the cell membrane marker β1 Na,K-ATPase was used. The intensity of each AE1 band relative to the total membrane fraction (β1 Na,K-ATPase signal) was quantified in each lane with NIH ImageJ software.

RESULTS

Model of AE1 Membrane-spanning Domain

Structural modeling of AE1 is problematic because of the absence of homologous structure available. Even the location of transmembrane segments is subject to controversy; the number and limits of transmembrane (TM) segments are dependent on the prediction tools used (see supplemental Table 1). The consensus is better in the N-terminal transmembrane domain from residue 398 to residue 728. In most cases, this domain encompasses eight transmembrane helices, but their length and precise location vary depending on the tool. The region from residue 730 to the end is much more variable with the number of helices ranging from 1 to 5. Similarly, prediction of inside/outside topology is also rather fuzzy. Altogether, these tools do not provide three-dimensional information (*i.e.* three-dimensional proximities of transmembrane segments) but help in considering alternative topologies. For predicting three-dimensional structures in the absence of clear homology, alternative

approaches are required. Therefore, we resorted to the I-TASSER method.

Among the five models proposed by I-TASSER, three of them were rather similar up to residue 850. These models are mostly based on the uracil transporter (Protein Data Bank code 3QE7). Model 2, based on the importin β subunit, was discarded because its topology was not compatible with most data available. Model 1 presented a topology based on the Na^+-glucose symporter and at first glance seemed of interest. Surprisingly, any tools we tested never retrieved the structural template suggested by Yamaguchi *et al.* (21), the bacterial chloride channel (Protein Data Bank code 1OTS). When the corresponding template (*Escherichia coli* chloride-proton exchanger (ClCA)) was imposed in I-TASSER, the resulting models did not respect the imposed topology, showing that the sequence-structure compatibility was not large enough to be imposed.

Hence, we mainly ended up with two different topologies. Model 1 is based on the Na^+-glucose symporter, and model 2 is based on the uracil transporter. Note that both are cation symporters. A careful inspection of model 1 showed that (i) the C-terminal end was extracellular and thus not compatible with experimental data and (ii) the location of Lys^{851} and Lys^{539} (intra- and extracellular, respectively) prevented their cross-linking by 4,4′-diisothiocyanostilbene-2,2′-disulfonate (DIDS) in disagreement with experimental data. Moreover, using alternative tools, we systematically retrieved the second template, *i.e.* Protein Data Bank code 3QE7. Supplemental Fig. 1 illustrates the structural alignment between AE1 transmembrane domain and uracil transporter (Protein Data Bank code 3QE7). In addition, the E-value and *p* value, which estimate the relevance of the alignment, led us to consider the proposed template. Hence, we focused on this model to identify helices forming the transport site.

We used the PPM server (22) to determine the limits of the transmembrane segments in the model (see supplemental Table 2). The topology of the model presents 12 transmembrane helical segments with two additional segments having a mixed structure, α-helix/coil. For convenience, the segments are numbered according to their predicted location in the membrane regardless of their secondary structure (Fig. 1).

There is a symmetry between TM4–5 and TM11–12, which form two inverted arches more or less of the same width. The helical parts of TM3 (in between TM4 and TM5) and TM10 (in between TM11 and TM12) point toward each other. TM1, TM2, and TM9 are located within the space delimited by TM4–5 and TM11–12. TM8 forms a long tilted helix spanning through this space parallel to the orientation of TM3 + TM10. TM6–7 and TM13–14 are arranged at the periphery of the structure. TM1–7 and TM8–14 structures are symmetrical (supplemental Fig. 2).

Note that the present model should be considered as a complementary tool to test new hypotheses and to guide experiments but should not be used to conduct intensive atomistic simulations. Nowadays, the tools, like QMEAN server, one of the most efficient tool available for assessing the accuracy of a structural model, are not appropriate to validate a transmembrane protein model (23). ProQM, the only tool available to assess membrane protein models, indicated that the quality of the model is medium (24). However, the present model provides useful information regarding helix spatial organization that should be further validated experimentally. The results detailed in the next sections strongly support the relevance of the model despite its low resolution.

Mutagenesis in TM5 and TM3

It has been shown that TM8 lines the anion exchange pathway of AE1. In the selected model, TM8 appears as a long tilted helix. Viewed from the top, the pathway along TM8 that was shown to drive anions partially faces TM5. Moreover, TM3 is in between the top of TM8 and TM5 (Fig. 1*B*). Thus, the possibility for TM8, TM5, and TM3 to be involved in the formation of AE1 transport site was investigated.

Putative TM5 contains a highly conserved amino acid sequence among anion exchangers SLC4A1, -A2, and -A3 ($F^{532}IYE^{535}$), and especially Ile^{533} is present in all known SLC4 anion exchangers (supplemental Fig. 3). Moreover, the anion exchanger inhibitor DIDS covalently binds to Lys^{539} at the top of this putative TM5. However, this lysine is not directly involved in the transport site (25). It is possible to cross-link Lys^{539} with Lys^{850} by DIDS, and this induces a covalent inhibition of anion exchange. The selected model places Lys^{539} and Lys^{850} in a position compatible with their cross-linking.

In putative TM3, sequence $G^{463}FSGPL^{468}$ is conserved in vertebrate SLC4A1, -A2, and -A3, and it has been proposed to correspond to one of the chloride binding sites of ClC (consensus sequence GSGIP) (26). To determine the role of TM5 and TM3 in AE1 transport activity, a cysteine-scanning mutagenesis combined with sulfhydryl-specific chemical labeling was done.

In TM5, residues Ser^{525}, Phe^{526}, Ile^{528}, Ser^{529}, Leu^{530}, Phe^{532}, Ile^{533}, Tyr^{534}, Glu^{535}, Phe^{537}, Lys^{539}, Leu^{540}, Ile^{541}, and Lys^{542} were changed one by one for cysteine. A similar approach was used to study the involvement of TM3 residues Ser^{465}, Leu^{468}, Phe^{471}, Glu^{472}, Glu^{473}, and Phe^{475}. Ser^{465} was substituted with cysteine, isoleucine, or alanine. This amino acid was proposed to correspond to Ser^{107} in Cl^- channels, which are involved in anion translocation. Leu^{468}, Phe^{471}, Glu^{472}, Glu^{473}, and Phe^{475} were substituted with cysteine. All mutants were expressed in *Xenopus* oocytes, and their correct addressing to oocyte plasma membrane was assessed by immunodetection of biotinylated AE1 on Western blots (supplemental Fig. 4).

The variation of AE1 expression level at the plasma membrane is fairly high as visualized by the large S.E. This discrepancy could be linked to differences between batches of oocytes, but it is also due to the calculation method. These bars show the ratio of chemiluminescence associated with overexpressed AE1 over that associated with the endogenous β1 subunit of the Na,K-ATPase. The large difference between these two signals emphasizes variations between experiments. Thus, it was not possible to establish statistically significant differences between mutants and WT AE1 with regard to their expression level except for S525C mutant in TM5 and S465A, E472C, and F475C in TM3 that were significantly less expressed than the WT AE1 in all experiments.

Transport Properties of the Mutants

Mutations in TM5—The anion exchange activity of cysteine mutants in TM5 was assessed. As shown by Fig. 2, all mutants were functional, *i.e.* able to exchange Cl^- and HCO_3^-, except for I528C, F532C, and E535C. In these three mutants, loss or strong reduction of anion exchange ability is not due to a reduced expression of the protein in oocyte plasma membrane (supplemental Fig. 4B). Only the S525C mutant exhibited a decreased

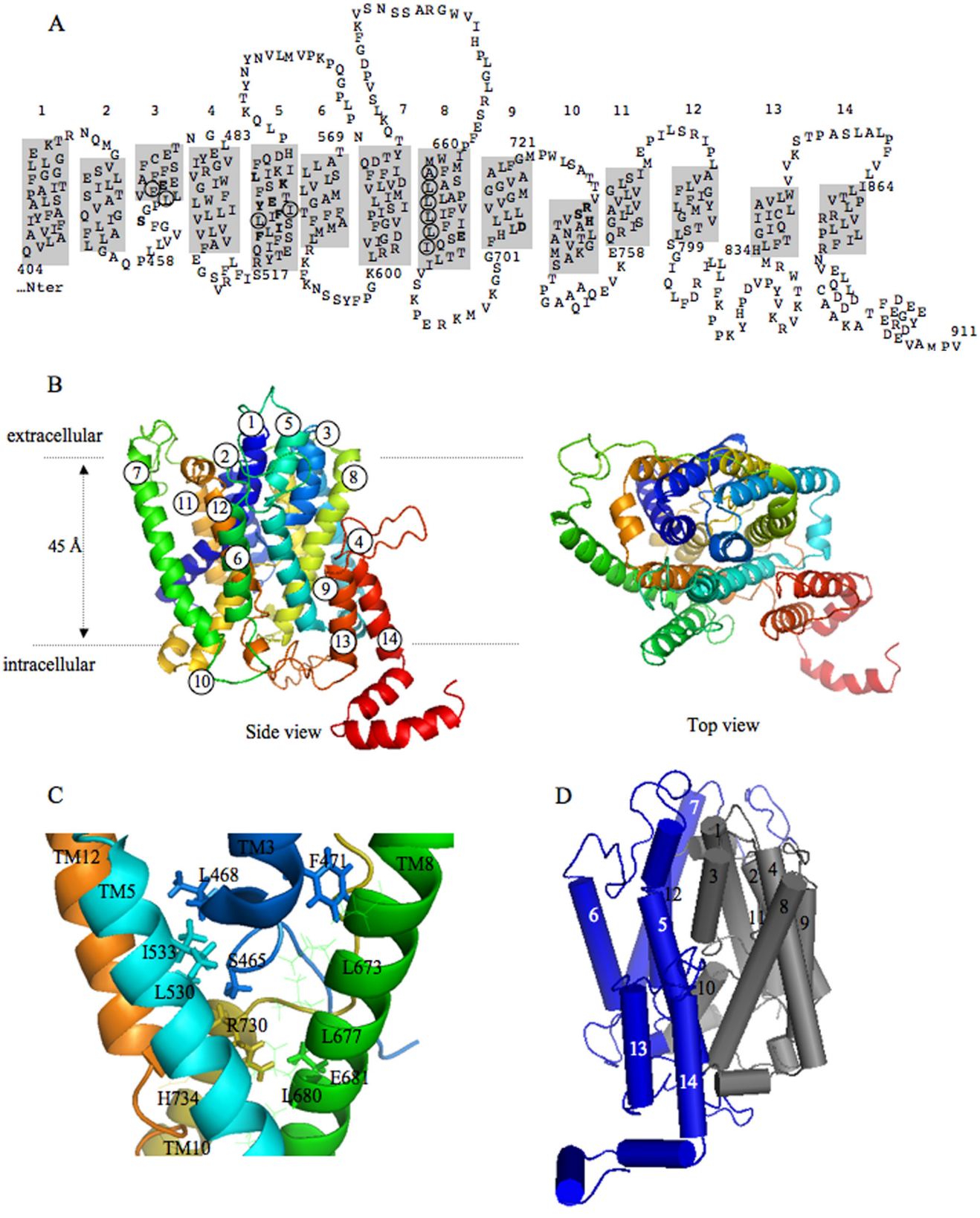

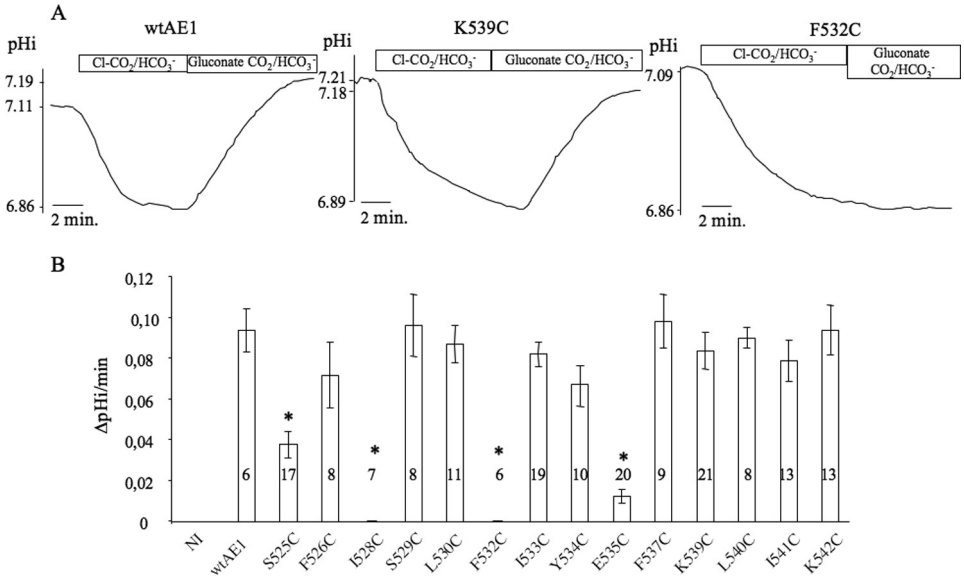

FIGURE 2. **Anion exchange of WT AE1 and cysteine mutants in TM5.** *A*, representative intracellular pH_i recordings in oocytes expressing WT AE1 and F532C and K539C mutants. Each trace comes from different experiments performed with different pH_i sensitive-electrodes. *wtAE1*, wild-type erythroid AE1. *B*, the ability of oocytes to recover from an acid load in CO_2/HCO_3^--buffered MBS was expressed as ΔpH_i/min. This corresponds to the initial slope of the curve recorded in medium without Cl^-. Data are means ± S.E. (*error bars*) of *n* (*number* in *bars*) oocytes from different batches (Student's *t* test; *, $p \leq 0.05$).

anion exchange activity that is correlated to a decreased expression level of the protein. Thus, S525C mutation does not impair AE1 transport features but rather decreases the amount of protein at the plasma membrane. As previous experiments have shown that some AE1 point mutations induced a Na^+ and K^+ leak, the cation permeability of oocytes expressing WT and mutated AE1 was also assessed.

Oocyte Na^+ and K^+ contents were measured after 3 days of AE1 expression (Fig. 3*A*). To be able to compare data from different batches of oocytes with varying basal Na^+ and K^+ contents in control oocytes (non-injected (NI)), results were expressed as the difference in Na^+ and K^+ contents between oocytes expressing WT or mutated AE1 and non-injected oocytes. We observed that mutations F526C, I528C, F532C, Y534C, K539C, and L540C induced a significant increase in Na^+ content correlated to a significant decrease in K^+ content. Considering S.E. values, only changes over 20% of cation contents were considered as significant. Thus, variations between NI and AE1-expressing oocytes below 10 μmol/g of dry weight are not significant. To confirm the faint cation leak for Y534C and K539C mutants, oocytes were incubated for 5 days in MBS with ouabain and bumetanide. In this case, $\Delta Na^+ = +26.6 \pm 8.6$ μmol/g d.w. and $\Delta K^+ = -21.1 \pm 4.5$ μmol/g d.w. for Y534C and $\Delta Na^+ = +22.8 \pm 6.3$ μmol/g d.w. and $\Delta K^+ = -27.6 \pm 5.7$ μmol/g d.w. for K539C. By contrast, E535C mutant did not leak Na^+ or K^+ after 5 days in MBS with ouabain and bumetanide.

The cation permeability was also assessed by Li^+ influx measurements (Fig. 3*B*). All the mutants able to change oocyte Na^+ and K^+ contents exhibited a significant Li^+ influx. The Li^+ influx measured in oocytes expressing E535C was slightly above control levels. However, this low increase in cation permeability was not associated with changes in Na^+ and K^+ content in contrast to L540C for which a low Li^+ influx was also detected. We did not further investigate the significance of the low Li^+ influx of E535C-expressing oocytes.

To assess whether TM5 lines the transport site, the anion exchange activity and the cation transport activity (when observed) were measured after binding of the following thiol reagents with different sizes and charges: MTSEA (cationic/neutral, 10:1 at pH 7.5), MTSET (cationic), MTSES (anionic), and PCMBS (anionic). We observed that PCMBS blocked anion exchange through L530C and I533C mutants (Fig. 4*A*) by 80 and 70%, respectively. Neither MTSEA nor MTSES at 5 mM inhibited anion exchange in oocytes expressing WT or cysteine mutants. For clarity, these data were not plotted in the figure. For the four mutants inducing a cation leak (F528C, F532C, Y534C, and K539C), Li^+ influx was insensitive to PCMBS, MTSET, and MTSEA.

FIGURE 1. **Human AE1 topology (*A*), three-dimensional model (*B*), and spatial organization of the transport domain (*C* and *D*).** *A*, topology of AE1 membrane-spanning domain deduced from the three-dimensional model. The *gray rectangles* represent α-helices spanning the membrane bilayer. *Circles* highlight residues that are along the ion pathway through the protein. Some amino acids that have been shown to be important for AE1 transport features are in *bold*: Glu^{681} in TM8; Asp^{705} in TM9; and Arg^{730}, Ser^{731}, and His^{734} in TM10 from previous publications and Ser^{465} in TM3 and Phe^{526}, Ile^{528}, Phe^{532}, Tyr^{534}, Glu^{535}, Lys^{539}, and Leu^{540} in TM5 from the present experiments. *B*, *dotted lines* indicate putative lipid bilayer width. The short size of TM13 and TM14 is similar to what is observed in uracil transporter UraA where they are halfway into the membrane. In the connecting loop between TM13 and TM14 lies the Lys^{851} that cross-reacts with Lys^{539} in the top part of TM3 through covalent binding to DIDS (the distance between the two lysines is compatible with the size of DIDS molecule, *i.e.* 20 Å). *C*, enlargement of the center for ion transport. Amino acids that have been experimentally shown to be involved in ion transport are highlighted: Leu^{468}, Phe^{471}, and Ser^{465} in TM3; Glu^{681} in TM8; Leu^{530} and Ile^{533} in TM5; and Arg^{730} and His^{734} in TM10. For clarity, only TM12-5-3-10 and TM8 are shown in this side view. In TM8, amino acids lining the ion transport site are also shown. *D*, extrapolation to AE1 of the functional organization of UraA. A core domain (*gray*) and a gate domain (*blue*) that associate with each other through hydrophobic interactions are shown. Figures were prepared with PyMOL. *Nter*, N terminus.

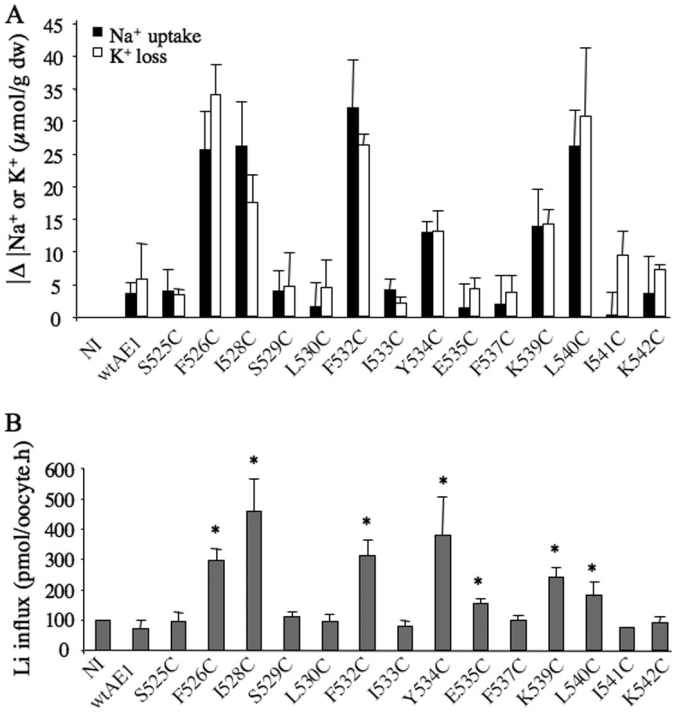

FIGURE 3. **Cation permeability of oocytes expressing WT AE1 and cysteine mutants in TM5.** *A*, intracellular Na^+ and K^+ were measured in oocytes 3 days after injection and incubation in MBS with ouabain and bumetanide. The variation in Na^+ and K^+ contents between control, NI oocytes, and AE1-injected oocytes was calculated for each experiment. The absolute value of these variations was averaged, and data are means ± S.E. (*error bars*) of three to six different experiments depending on mutants. The mean value for Na^+ content in NI oocytes is 50.1 ± 4.5 μmol/g d.w. (n = 14). The mean value for K^+ content in NI oocytes is 59.2 ± 5.5 μmol/g d.w. (n = 14). *wtAE1*, wild-type erythroid AE1. *B*, Li^+ influx ratio in oocytes expressing WT AE1 and cysteine mutants. To be able to compare experiments with varying basal Li^+ influx in NI oocytes (from a minimum of 42 to a maximum of 250 pmol/h·oocyte depending on oocyte batches; mean, 139 ± 20 pmol/h·oocyte; n = 15 independent experiments), Li^+ influxes in oocytes expressing WT or mutated AE1 were normalized to the basal Li^+ influx in each experiment. Data are expressed as percentage of NI as means ± S.E. (*error bars*) of three (WT AE1, S525C, F526C, S529C, L530C, I533C, F537C, L540C, I541C, and K542C), five (F532C and K539C), or seven (I528C, Y534C, and E535C) different experiments (Student's *t* test; *, $p \leq 0.05$).

Mutations in TM3—Fig. 4*B* illustrates the anion exchange activity of mutants in TM3. S465C, S465A, L468C, F471C, and F475C were still able to exchange Cl^- and bicarbonate. By contrast, S465I and E472C abolished anion exchange activity, whereas E473C drastically reduced anion exchange activity. E472C was hardly detectable at the plasma membrane; thus, it is not possible to make conclusions about the effect of this mutation on anion exchange activity *per se* (supplemental Fig. 3C). S465I and E473C on the other hand were expressed at the plasma membrane, and the lack of anion exchange activity of these mutants points to a role for Ser^{465} and Glu^{473} in the transport process. The effect of PCMBS binding to cysteine mutants in TM3 was then assessed. This reagent strongly decreased anion exchange of L468C and F471C mutants (Fig. 4*B*). None of the substitutions on TM3 residues induced a cation leak (evaluated by cation content after 3 days in MBS with ouabain and bumetanide).

Involvement of TM5 and TM3 in Cation-leaky AE1—In previous studies, it was shown that H734R mutation converted the anion exchanger into a cation conductance (5). The H734R mutation is associated with a hereditary stomatocytosis (9). The question arises as to whether the cation leak induced by H734R mutation was sensitive to cysteine mutations in TM5 or TM3 and whether this cation leak could be blocked by sulfhydryl reagents binding cysteine in TM5 or TM3.

The following double mutants, H734R and cysteine substitutions in TM5 that did not induce a cation leak *per se*, were constructed: S525C/H734R, S529C/H734R, L530C/H734R, I533C/H734R, E535C/H734R, F537C/H734R, L540C/H734R, I541C/H734R, and K542C/H734R. Moreover, another double mutant, F526C/H734R, a Cys mutant able to induce a cation leak, was also constructed. The Li^+ influx induced by H734R mutations alone is greater than the Li^+ influx induced by single cysteine mutations in TM5 (Fig. 5*A* compared with Fig. 3*B*). Moreover, we observed that an additional cysteine substitution in H734R mutant at the following positions increased the Li^+ influx: F526C, S529C, F537C, L540C, and I541C. The greater Li^+ permeability of F526C/H734R, S529C/H734R, F537C/H734R, L540C/H734R, and I541C/H734R double mutants is not explained by a higher amount of protein at the plasma membrane (supplemental Fig. 5).

The effect of chemical reagent binding on accessible cysteine was then assessed on these double AE1 mutants. Oocytes expressing AE1 H734R/Cys double mutants in TM5 were treated with MTSET, MTSEA, or PCMBS prior to Li^+ influx measurement. Fig. 5*B* shows that two positions, Cys^{530} and Cys^{533}, were affected by MTSET and/or PCMBS treatment in H734R mutant. MTSET inhibited by 25% Li^+ influx of oocytes expressing L530C/H734R mutant, whereas PCMBS and MTSET inhibited by 45 and 33%, respectively, Li^+ influx of oocytes expressing I533C/H734R. As MTSEA (5 mM) did not significantly change Li^+ influx of any double mutants, these results were not plotted in Fig. 5 to avoid confusion.

Thus, positions Cys^{533} and Cys^{530} are both accessible in the anion exchange conformation of WT AE1 and in the cation leaky conformation of H734R mutant. Moreover, they are involved in the anion exchange activity as well as in the cation leak.

As it was observed that PCMBS blocked anion exchange of two cysteine mutants in TM3 (L468C and F471C), the involvement of these two positions in the cation leak induced by H734R mutation was also assessed. Moreover, the involvement of Ser^{465} was also checked on cation leak induced by H734R mutation. Double mutants L468C/H734R, F471C/H734R, and S465I/H734R were constructed, and their expression level at the plasma membrane was not significantly different from that of WT AE1 (supplemental Fig. 5). Fig. 6 illustrates the Li^+ influx of L468C/H734R, F471C/H734R, and S465I/H734R constructs. This influx was not inhibited by 1 mM PCMBS or 10 mM MTSET treatment. Remarkably, a strong reduction of Li^+ influx was observed in oocytes expressing S465I/H734R mutants, suggesting the importance of Ser^{465} in the cation leak induced by H734R mutation.

DISCUSSION

The goals of the present experiments were to identify the ion transport site within AE1 membrane-spanning domain and to propose a spatial organization of this domain. The AE1 model is

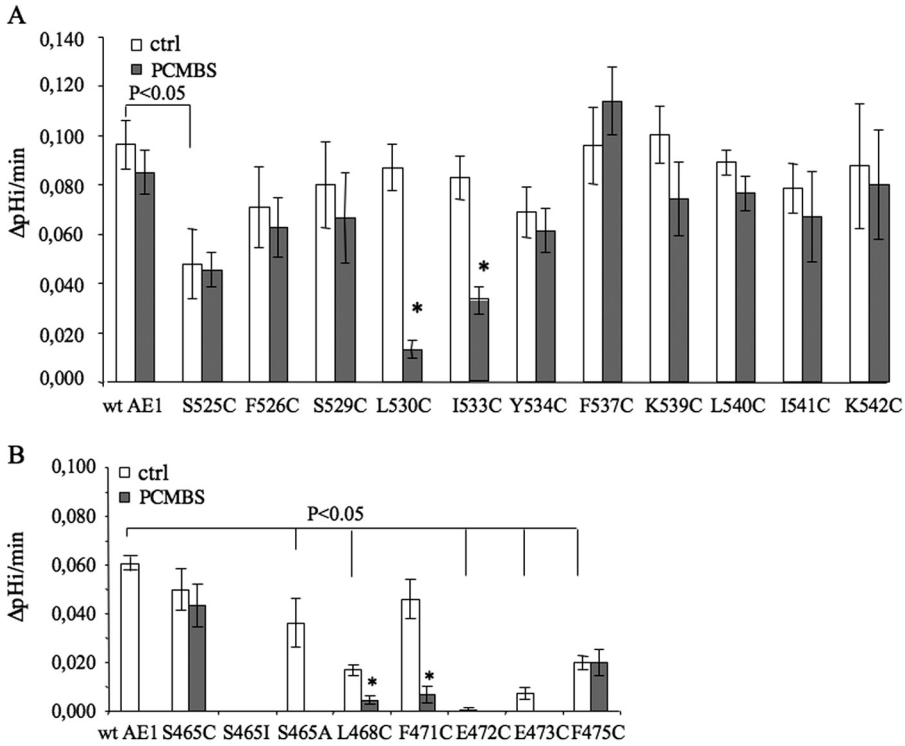

FIGURE 4. **Effect of PCMBS on anion exchange activity of WT and mutated AE1.** *White bars* represent control condition. *Gray bars* represent pH_i recovery of oocytes treated for 15 min with 1 mM PCMBS prior to intracellular pH recording. Data are means ± S.E. (*error bars*) of 10 oocytes from different experiments. The control (*ctrl*) condition and sulfhydryl reagent condition were recorded on oocytes from the same batch of injection (Student's *t* test between control and PCMBS condition; *, $p \leq 0.05$). *A*, cysteine substitutions in TM5. *B*, amino acid substitutions in TM3. The different level of WT AE1 anion exchange activity between *A* and *B* could reflect the different periods of time at which the experiments on TM3 and TM5 mutants were done. The mean ΔpH_i/min for WT AE1 is 0.063 with a standard error of 0.030 ($n = 41$ recordings over 2 years).

based on the structure of UraA, the uracil-H^+ cotransporter (27). At first glance, this result is unexpected for an electroneutral anion exchanger, which is more likely compared with chloride channel family members. Indeed, a recent interpretation of electron density maps of AE1 crystals proposed some similarities with Cl^- channel structure (21). Some long and tilted helices could be identified in AE1 crystals, and two V-shaped densities inserted into the membrane from opposite sides were also identified. These V-shaped helices are found in Cl^- channel structure (28). However, V-shaped helices are also found in H^+ or Na^+ symporters. In addition, amino acid sequence similarity between AE1 membrane-spanning domain and UraA or ClCA does not favor the chloride channel, these sequences are quite similar. Nevertheless, although all the tools we used failed to identify ClCA as an appropriate template, we built homology models using two different alignments. Whatever the alignments, the results did not match available functional and topological data. For instance, residues Leu^{530}, Ile^{533}, Leu^{669}, Leu^{673}, Leu^{468}, and Phe^{471} shown to influence transport properties were far away in the models based on ClCA. The region from Arg^{808} to Leu^{835} that was shown to be intracellular on the basis of antibody recognition (42) is exposed to the extracellular medium in the model based on ClCA. All these results tend to confirm that that UraA template would be more appropriate.

It should be noted that UraA structure is also a double funnel shape structure related by an internal 2-fold symmetry. This kind of structure, observed in Na^+ symporters for example, allows transport of many different solutes: amino acids, sugar, nucleobase, glycerol, and water with H^+, Na^+, K^+, and/or Cl^- ions (28–31). As mentioned previously, AE1 is able to transport amino acids, urea, Na^+, and K^+ and form an anion conductive pathway in trout erythrocytes (5, 12, 13, 15, 16). Point mutations convert the electroneutral human AE1 into a Na^+ and K^+ conductance (5). To some extent, AE1 shows transport similarities with the glutamate transporter, an anion channel with glutamate, Na^+, and K^+ permeability, that has a structure related to Na^+-coupled transporters (29).

The three-dimensional AE1 model presents 14 transmembrane segments arranged into two structural repeats, TM1–7 and TM8–14 (supplemental Fig. 2). The N-terminal and C-terminal parts are cytoplasmic. As for UraA, two transmembrane segments are partly helical, TM3 and TM10, and these two half-helices are superimposed. In UraA, these semihelical membrane -spanning segments are crucial for uracil binding and present a short β-strand that is not observed in the AE1 model. Similar discontinuous helices symmetrically related are also observed in neurotransmitter-, amino acid-, and sugar-sodium symporters and account for substrate binding (32). As shown in Fig. 1*B*, *Top view*, AE1 membrane-spanning domain can be divided into two parts: the transmembrane segments 1-2-3-4-8-9-10 and 11 on one hand and the transmembrane segments 5-6-7-12-13 and 14 on the other hand. The relevance of the proposed three-dimensional structure for AE1 can be assessed by comparison with the available data accumulated over more than 50 years to describe AE1 topology and functioning.

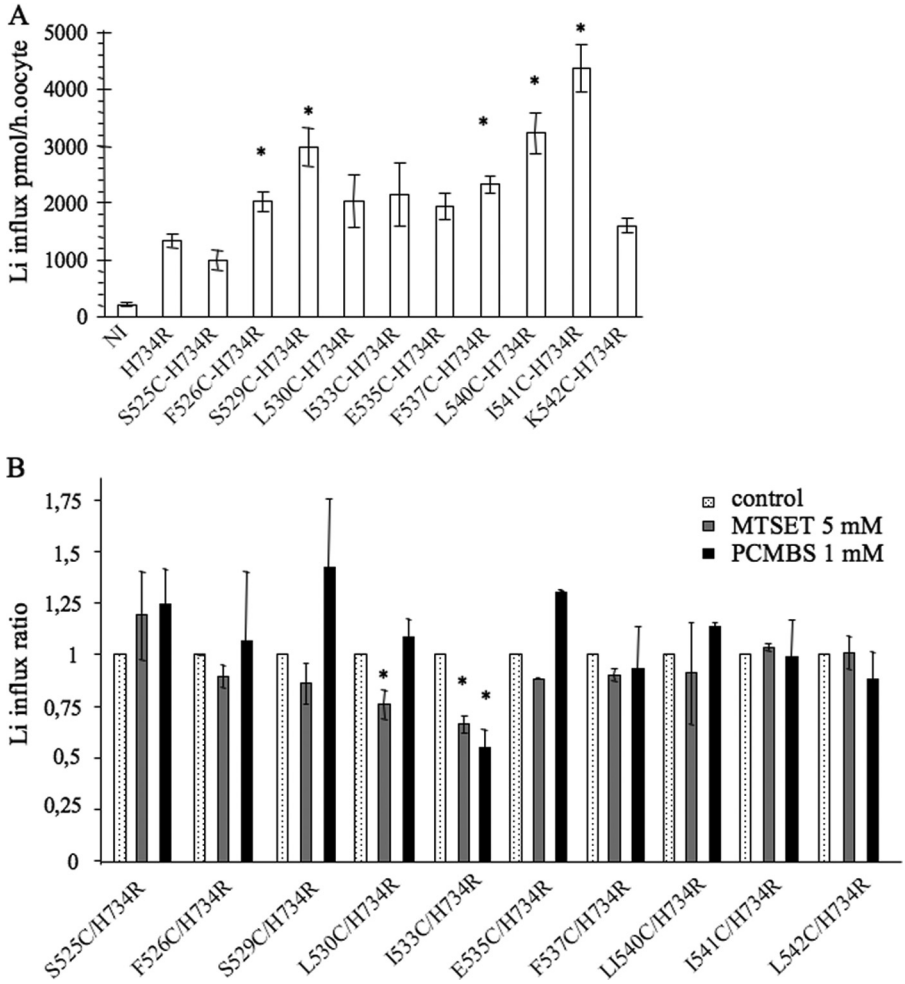

FIGURE 5. **Li^+ influx in oocytes expressing cation-leaky AE1.** *A*, Li^+ influx in oocytes expressing H734R mutant and H734R/Cys double mutants in TM5. Data are means ± S.E. (*error bars*) of three to five different experiments. *B*, effect of sulfhydryl reagents on Li^+ influx induced by expression of H734R/Cys double mutants in TM5. For each experiment, the Li^+ influx for control condition was set at 100 pmol/h·oocyte, and Li^+ influx in MTSET- (0.5 mM) or PCMBS (1 mM)-treated oocytes was normalized to this value. Data are means ± S.E. (*error bars*) of three different experiments (Student's *t* test; *, $p \leq 0.05$).

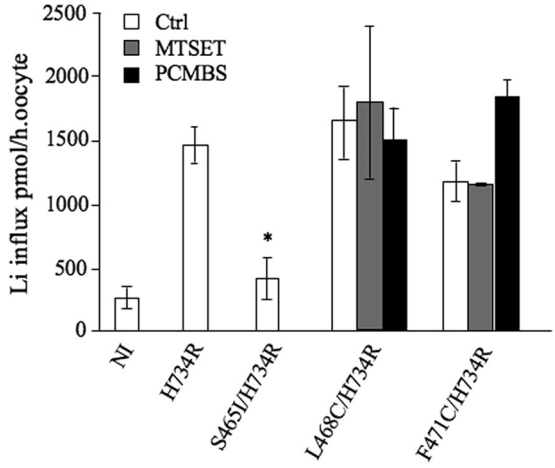

FIGURE 6. **Li^+ influx in oocytes expressing double mutants (H734R and point mutations in TM3).** Data are means ± S.E. (*error bars*) of three different experiments (Student's *t* test; *, $p \leq 0.05$). Only oocytes expressing L468C/H734R and F471C/H734R were treated with PCMBS (1 mM) or MTSET (5 mM). *Ctrl*, control.

A great number of experiments have been carried out to determine AE1 topology. These data have led to two different propositions: one with 13 α-helices and a loop connecting the extracellular C-terminal part of α-helix 11 and the intracellular N-terminal part of α-helix 12 and one with 14 α-helices (33–37). These two topologies differ mainly after TM9 (Gly^{714}) with either five α-helices spanning the lipid bilayer or four α-helices with a re-entrant loop between α-helix 11 and 12 (residues 808–835). In our model, TM10 (residues Pro^{722} to Gln^{752}) corresponds to a transmembrane segment. Experimental evidence has long questioned the sidedness of this region. The amino acids in this region have been proposed to form an extracellular loop on the basis of *N*-glycosylation-scanning mutagenesis in a cell-free system or in transfected cells. Cysteine-scanning mutagenesis also favored this orientation (37). However, in this domain, Lys^{743} was shown to be accessible from the extracellular side or intracellular side depending on the kind of experiments (38, 39). Kanki *et al.* (40) have proposed an explanation to these contradictory observations, and they concluded that during synthesis this region is accessible from the extracellular side, and it is later occluded within the AE1 molecule. This sequestration requires TM1–3 and TM11. In the present model, this domain forms a transmembrane span (TM10) that is in accordance with the experiments of Kuma *et al.* (41) showing

TABLE 1

Summary of experimental data

For plasma membrane immunodetection, ++ refers to the immunodetection level of WT AE1, and + indicates that the protein was immunodetected at a lower level than WT. All constructs were immunodetected. For anion exchange activity, there were five levels of signal ranging from +++ to −− (no signal at all). +++ refers to anion exchange activity of WT AE1, − indicates very faint signal (0.01 ΔpH_i/min), + indicates anion exchange activity around 0.02 ΔpH_i/min, and ++ indicates that anion exchange activity was reduced by about half compared with WT. For Na^+ and K^+ leak, + indicates the presence of cation leak, and − indicates the absence of cation leak.

AE1 amino acid substitutions	Plasma membrane immunodetection	Anion exchange activity	Na^+ and K^+ leak	Transport sensitivity to thiol alkylation
WT AE1	++	+++	−	None
TM3				
S465C	++	+++	−	None
S465I	++	−−	−	None
S465A	+	++	−	None
L468C	++	+	−	PCMBS
F471C	++	+++	−	PCMBS
E472C	+	−−	−	None
E473C	++	−	−	None
F475C	+	+	−	None
TM5				
S525C	+	++	−	None
F526C	++	+++	+	None
I528C	++	−−	+	None
S529C	++	+++	−	None
L530C	++	+++	−	MTSET (cation transport), PCMBS (anion transport)
F532C	++	−−	+	None
I533C	++	+++	−	PCMBS (anion and cation transport), MTSET (cation transport)
Y534C	++	+++	+	None
E535C	++	−	−	None
F537C	++	+++	−	None
K539C	++	+++	+	None
L540C	++	+++	+	None
I541C	++	+++	−	None
K542C	++	+++	−	None

that Lys^{743} is cleaved by intracellular proteases but not by extracellular proteases in red cells.

The next two TMs, TM11 and TM12, are therefore oriented in the opposite direction compared with the topology proposed by Zhu *et al.* (33), and the long loop between TM12 and TM13 (Arg^{808} and Leu^{835}) is intracellular. Wainwright *et al.* (42) have shown that this loop corresponds to an intracellular loop on the basis of antibody recognition (BRIC 132).

The controversy regarding the topology of the two regions corresponding roughly to residues 720–760 and 808–835 has recently been summarized by Hirai *et al.* (43). They proposed two different topologies of AE1 (a and b) combining published data and their analysis of the electron density maps of AE1 crystals. Our present model favors the topology called b with region 720–760 forming a transmembrane segment and region 808–834 being an intracellular loop connecting TM12 and TM13. Moreover, this model fits nicely with the working model proposed by Groves and Tanner (35). By co-expressing pairs of complementary fragments of AE1 combined with co-immunoprecipitation in non-denaturizing detergent solutions, they suggested that the core of the protein might comprise two subdomains containing the closely interacting TM spans 1–5 and TM spans 9–12. The region containing TM spans 6–7 and 13–14 were proposed to be at the periphery of the core structure. In addition, it has been shown that deletion of TM6 and TM7 from full-length AE1 does not prevent anion exchange activity (12). However, this deletion changes AE1 transport features because the protein develops an anion conductance in place of an anion exchange. Thus, these two TMs are not required for anion exchange but impose the electroneutral transport behavior of anion exchange. Two AE1 point mutations, R589H and S613F, associated with distal renal tubular acidosis are located in TM6 and TM7, and they induce a cation leak in a still functional anion exchanger (7). TM6 and TM7 are not part of the ion path but probably participate in connecting TMs involved in this function.

It is possible to reconstitute a functional anion exchanger by co-expressing two independent cDNAs, one coding for the N-terminal part of the protein until the end of putative TM5 and one coding for the C-terminal part of the protein starting in putative TM6 (35). This suggests that the first five membrane-spanning helices adopt a three-dimensional functional structure independently of the next TM segments. Moreover, it has been shown that cutting this structure after putative TM4 did not allow recovery of a functional anion exchanger. Thus, the control of TM5 position by its link to TM4 appears to be essential for anion exchange activity.

The model shows that TM3 and TM5 share contacts with TM8, which has been proposed to line the anion exchange pathway. Thus, it was hypothesized that TM3 and TM5 could be involved in the AE1 transport site, and cysteine-scanning mutagenesis was done on conserved positions of these segments. The results of amino acid substitutions in TM3 and TM5 are summarized in Table 1.

Among known sequences of anion exchangers (SLC4A1, -A2, and -A3), there is a conserved consensus sequence in TM3: G^{463}F(S/T)GP(L/V)(L/M)(L/V)F(E/D)E^{473}A(F/Y/L)(F/Y/N/M)XF(C/S)^{479}. In the model, the helical part of TM3 starts at Val^{470}. Substitutions S465I and E473C abolished the anion exchange activity, whereas thiol reagent binding on L468C and F471C mutants prevented anion exchange, thus showing the involvement of TM3 in transport activity of AE1. In addition,

some mutations are probably responsible for AE1 misfolding as shown by reduced immunodetection at the plasma membrane of S465A, E472C, and F475C mutants. In zebra fish, the retsina mutation corresponding to E472G substitution leads to the absence of anion exchanger in erythrocyte membrane (44). Altogether, these results indicate the importance of Glu^{472} in TM3 for proper folding of AE1 and probably of all anion exchangers because this Glu is highly conserved (it could be an Asp in invertebrates). Moreover, Ser^{465} also appears to be important for AE1 folding because its substitution by Ala led to a lower detection of the protein at the plasma membrane. However, this protein was still able to exchange anions. Thus, a polar residue does not seem important in position 465 for anion exchange activity. The size of the lateral chain is probably more important because S465I mutation prevented the anion exchange activity of AE1 without impairing protein expression. Further studies simulating the effects of amino acid substitutions on the model would help to better understand how Ser^{465} is involved in the transport mechanism and folding of the protein. Another amino acid substitution in TM3 of human AE1, C479W, was shown to impair AE1 trafficking to the plasma membrane as well as anion exchange activity (45).

Thus, our present results confirm the role of TM3 in AE1 folding and show in addition its involvement in anion exchange activity. Especially residues Ser^{465}, Leu^{468}, Phe^{471}, and Glu^{473} appear to play a role in anion translocation. Further experiments should be done to better understand how these amino acids are involved in the transport process.

Cysteine-scanning mutagenesis in TM5 showed that mutants L530C and I533C react with thiol reagents, which prevent anion exchange. This suggests that these residues are involved in anion access to the AE1 transport site. Unlike Ile^{533}, which is conserved in the family of anion exchangers, Leu^{530} can be substituted with other non-polar residues (Ala in skate AE3 and Val or Phe in invertebrate AE).

It is not possible to block anion exchange with thiol reagent binding to positions below Leu^{530} and above Ile^{533} along a line facing the space between TM5–3 and TM8. This could be interpreted either as limited access of the reagent to these positions or as an absence of blocking of the anion exchange when bound. This interpretation suggests that access to the transport site is too large above Ile^{533} to be blocked by PCMBS, which is 9 Å long with the thiol function (6.5 Å alone). Thus, the transport site should narrow below Ile^{533}. The model shows that the distance between TM5 and TM8 narrows between the facing residues Ile^{533} in TM5 and Leu^{673} in TM8 (6.5 Å), which is compatible with the blocking effect of PCMBS binding to Cys^{533} as well as to Cys^{673} in TM8 (19). Another interpretation of PCMBS blocking could be that its binding to TM5 prevents helix movements involved in transport process.

We observed that some substitutions of amino acids in TM5 are associated with changes in AE1 transport features. E535C dramatically reduced anion exchange activity. I528C and F532C mutations abolished the anion exchange activity and induced a cation leak. F526C, Y534C, K539C, and L540C mutations did not prevent anion exchange but induced a cation leak. The Na^+ and K^+ gradients were dispelled by a ouabain- and bumetanide-insensitive pathway. Thus, some positions in TM5 are crucial for AE1 transport features. It was already known that either AE1 could be converted into a cation conductance or that a cation conductance could be observed in a still functional anion exchanger. These peculiar transport features result from specific point mutations in the transmembrane domain (such as H734R in TM10), and some of these point mutations are associated with hereditary red cell or renal diseases (5, 7–10, 46). Our present results extend to TM5 the list of amino acids that, when substituted in AE1, induce a Na^+ and K^+ leak in *Xenopus* oocytes. With F526C, Y534C, K539C, and L540C mutations, AE1 carries anion exchange and cation leak activities. With I528C and F532C mutations, there is no more anion exchange activity; the exchanger is converted into a cation leak.

The intensity of the cation leak induced by cysteine substitutions in TM5 is weak compared with the cation leak induced by H734R single mutation (for H734R-expressing oocytes, the Li^+ influx is about 15 times higher than the control, whereas for cysteine mutants in TM5, it is between 2 and 4 times higher than the control). Differences in the expression levels of the proteins in oocyte plasma membrane do not account for this observation. This should rather mean that the cation pathway induced by H734R mutation is more permeable than that induced by cysteine substitutions in TM5. The fact that different point mutations lead to varying intensities of the ouabain- and bumetanide-insensitive cation leak but similar plasma membrane protein content favors the hypothesis of a leak through AE1 rather than through an endogenous transporter. Moreover, some cysteine substitutions in TM5 were able to increase the cation leak of H734R mutant, corroborating the involvement of TM5 in cation permeability.

The question of a unique transport pathway in AE1 accounting for anion exchange and/or cation leak has been addressed in a previous publication (11). It was observed that thiol reagent binding on cysteine residues in TM8 could block anion exchange on WT AE1 or cation leak in H734R point-mutated AE1. The present results with L530C and I533C substitutions in H734R AE1 show that the cation leak could be partly blocked by PCMBS binding on Cys^{530} or Cys^{533}. Consequently, like TM8, TM5 participates in the anion exchange activity of WT human AE1 and in the cation leak activity of point-mutated H734R AE1. However, cation leak inhibition is lower than anion transport inhibition (Figs. 5*B* and 4*A*). This suggests that in H734R-mutated AE1 a path still large enough with PCMBS binding on Cys^{530} or Cys^{533} accounts for some Li^+ transport.

The similarity between uracil transporter UraA and the AE1 model suggests that the two proteins should share a common transport mechanism. The uracil transporter UraA is organized into a core domain (TM1–4 and TM8–11) and a gate domain (TM5–7 and TM12–14). The interface between these two domains involves hydrophobic contacts of TM5 and TM12 in the gate domain with TM3–8 and TM10 in the core domain. The substrate binding site is located in a pocket formed at the junction of TM3 and TM10 α-helical parts. In this pocket, uracil is coordinated with residues in TM8 (Glu^{241} and His^{245}), TM3 (Phe^{73}), TM10 (Gly^{289} and Glu^{290}), and TM12 (Tyr^{342}) (27). UraA is a proton-coupled symporter. It is proposed that substrate-free UraA is outward-open with the two negative charges of Glu (241 and 290) preventing closure of the gate

domain onto the core domain. The proton is translocated from Glu^{241} or Glu^{290} to His^{245}, and this translocation induces a rotation of the gate domain around the bound uracil. Then transporter conformation changes from outward-open to inward-open. Along TM8, substitution of Glu^{241} or His^{245} by an Ala abolished uracil transport.

It is noteworthy that, in AE1, TM8 also lines the AE1 transport site (19), and along this helix, Glu^{681} is involved in the electroneutral anion exchange activity of the protein (18). There is 62% similarity between UraA TM8 and AE1 TM8 primary sequences, and the size of the helices is the same. The two Glu residues important for protein function are not at the same level along the helix: Glu^{681} in AE1 is one helix turn lower than Glu^{241} in UraA TM8 (supplemental Fig. 6). Glu^{681} in AE1 was proposed to lie within the transport pathway and to be alternatively exposed to the intracellular and extracellular media (18, 47, 48). Interestingly, Glu^{681} in the present model is in the vicinity of residues His^{734}, Ser^{731} (in TM10), and Asp^{705} (in TM9). Point mutations leading to H734R, S731P, and D705Y substitutions (responsible for hereditary stomatocytosis) block anion exchange and induce a cation conductance in AE1 (5, 9). The work from Zaki *et al.* (47) has shown that two arginyl residues in AE1 membrane-spanning domain are involved in the anion binding site. These arginines were identified as Arg^{490} (extremely conserved residue in SLC4) and Arg^{730} (conserved in SLC4A1, -A2, and -A3). In our model, the side chain of Arg^{490} in TM4 protrudes toward the helical part of TM3, whereas Arg^{730}, located at the beginning of the TM10 helical part, faces Glu^{681} in TM8 (Fig. 1*C*). Arg^{730} in AE1 TM10 corresponds to Glu^{290} in UraA TM10. These residues in their respective transporter are deeply involved in the transport activity of the proteins. E290A substitution in UraA abolishes uracil transport, whereas R730C substitution abolishes anion exchange activity of AE1 (49).

In addition to TM8, TM3 might also be involved in the AE1 transport pathway as it is in uracil transporter. Phe^{471} was shown to be accessible to thiol reagent blocking when substituted with a cysteine. In UraA, a Phe (Phe^{73}) is also found in a similar position along TM3 (supplemental Fig. 6). This Phe^{73} can be substituted with an Ala without impairing uracil transport; however, this bulky residue together with His^{245} in TM8 is proposed to insulate substrate from the outside environment. Finally, TM5 appears to face the AE1 transport pathway and to control the size or the shape of this passage. Positions Phe^{528}, Leu^{530}, and Ile^{533} in AE1 correspond to Ile^{132}, Leu^{136}, and Val^{139}, respectively, in UraA. In UraA, these residues mediate interaction of the gate domain with the core domain. In the upper part of AE1 TM5, Tyr^{534}, Phe^{537}, Lys^{539}, and Lys^{542} face Leu^{468}, Glu^{472}, Glu^{473}, and Phe^{475} in TM3. Substitutions on most of these residues were shown to affect anion exchange activity. This suggests that these contacts are required for proper functioning of AE1.

According to UraA transporter functioning and similarities between UraA and AE1 regarding amino acids crucial for transport, it could be proposed that the extracellular side of TM1, TM2, TM3, TM8, and TM9 should circumscribe the AE1 outside vestibule, providing access for the extracellular medium. The intracellular part of TM5, TM8, TM10, and TM12 with the loop connecting TM12 and TM13 should circumscribe the inside vestibule, providing access for the intracellular medium. A core domain consisting of TM1, TM2, TM3, TM4, TM8, TM9, TM10, and TM11 would interact with a gate domain (TM5, TM6, TM7, TM12, TM13, and TM14) (Fig. 1*D*). A tilt of the gate domain should open and close the extracellular medium access to the transport binding site formed around the helical extremities of TM3 and TM10.

AE1 structure should enable anion exchange by a movement of the protein that is compatible with the opening of a leak for Na^+ and K^+. The present three-dimensional model provides a useful basis to design further experiments to understand how a unique ion pathway within AE1 protein could exchange anions and/or leak cations. The model could help identification of helices in AE1 crystals, and it is a starting point to model point mutations and to study their involvement in the organization and functioning of the transport domain *in silico* and *in vivo*.

Acknowledgment—We are grateful to Dr. Céline Feillet for precious help in editing the manuscript and helpful comments.

REFERENCES

1. Bamberg, E., and Passow, H. (eds) (1992) *The Band 3 Proteins: Anion Transporters, Binding Proteins and Senescent Antigens*, Elsevier, Amsterdam, Netherlands
2. Chu, H., and Low, P. S. (2006) Mapping of glycolytic enzyme-binding sites on human erythrocyte band 3. *Biochem. J.* **400,** 143–151
3. Lindenthal, S., and Schubert, D. (1991) Monomeric erythrocyte band 3 protein transports anions. *Proc. Natl. Acad. Sci. U.S.A.* **88,** 6540–6544
4. Pucéat, M., Korichneva, I., Cassoly, R., and Vassort, G. (1995) Identification of band 3-like proteins and Cl^-/HCO_3^- exchange in isolated cardiomyocytes. *J. Biol. Chem.* **270,** 1315–1322
5. Guizouarn, H., Martial, S., Gabillat, N., and Borgese, F. (2007) Point mutations involved in red cell stomatocytosis convert the electroneutral anion exchanger 1 to a nonselective cation conductance. *Blood* **110,** 2158–2165
6. Ellory, J. C., Guizouarn, H., Borgese, F., Bruce, L. J., Wilkins, R. J., and Stewart, G. W. (2009) Review. Leaky $Cl^-HCO_3^-$ exchangers: cation fluxes via modified AE1. *Philos. Trans. R. Soc. Lond. B Biol. Sci.* **364,** 189–194
7. Walsh, S., Borgese, F., Gabillat, N., Unwin, R., and Guizouarn, H. (2008) Cation transport activity of anion exchanger 1 mutations found in inherited distal renal tubular acidosis. *Am. J. Physiol. Renal Physiol.* **295,** F343–F350
8. Walsh, S., Borgese, F., Gabillat, N., and Guizouarn, H. (2009) Southeast Asian AE1 associated renal tubular acidosis: cation leak is a class effect. *Biochem. Biophys. Res. Commun.* **382,** 668–672
9. Bruce, L. J., Robinson, H. C., Guizouarn, H., Borgese, F., Harrison, P., King, M. J., Goede, J. S., Coles, S. E., Gore, D. M., Lutz, H. U., Ficarella, R., Layton, D. M., Iolascon, A., Ellory, J. C., and Stewart, G. W. (2005) Monovalent cation leaks in human red cells caused by single amino-acid substitutions in the transport domain of the band 3 chloride-bicarbonate exchanger, AE1. *Nat. Genet.* **37,** 1258–1263
10. Iolascon, A., De Falco, L., Borgese, F., Esposito, M. R., Avvisati, R. A., Izzo, P., Piscopo, C., Guizouarn, H., Biondani, A., Pantaleo, A., and De Franceschi, L. (2009) A novel erythroid anion exchange variant (Gly796Arg) of hereditary stomatocytosis associated with dyserythropoiesis. *Haematologica* **94,** 1049–1059
11. Barneaud-Rocca, D., Borgese, F., and Guizouarn, H. (2011) Dual transport properties of anion exchanger 1: the same transmembrane segment domain is involved in anion exchange and in a cation leak. *J. Biol. Chem.* **286,** 8909–8916
12. Parker, M. D., Young, M. T., Daly, C. M., Meech, R. W., Boron, W. F., and Tanner, M. J. (2007) A conductive pathway generated from fragments of

the human red cell anion exchanger AE1. *J. Physiol.* **581,** 33–50
13. Guizouarn, H., Gabillat, N., Motais, R., and Borgese, F. (2001) Multiple transport functions of a red blood cell anion exchanger, tAE1: its role in cell volume regulation. *J. Physiol.* **535,** 497–506
14. Garcia-Romeu, F., Borgese, F., Guizouarn, H., Fiévet, B., and Motais, R. (1996) A role for the anion exchanger AE1 (band 3 protein) in cell volume regulation. *Cell. Mol. Biol.* **42,** 985–994
15. Fiévet, B., Gabillat, N., Borgese, F., and Motais, R. (1995) Expression of band 3 anion exchanger induces chloride current and taurine transport: structure-function analysis. *EMBO J.* **14,** 5158–5169
16. Fiévet, B., Perset, F., Gabillat, N., Guizouarn, H., Borgese, F., Ripoche, P., and Motais, R. (1998) Transport of uncharged organic solutes in *Xenopus* oocytes expressing red cell anion exchangers (AE1s). *Proc. Natl. Acad. Sci. U.S.A.* **95,** 10996–11001
17. Jennings, M. L. (1976) Proton fluxes associated with erythrocyte membrane anion exchange. *J. Membr. Biol.* **28,** 187–205
18. Jennings, M. L., and Smith, J. S. (1992) Anion-proton cotransport through the human red blood cell band 3 protein. Role of glutamate 681. *J. Biol. Chem.* **267,** 13964–13971
19. Tang, X. B., Kovacs, M., Sterling, D., and Casey, J. R. (1999) Identification of residues lining the translocation pore of human AE1, plasma membrane anion exchange protein. *J. Biol. Chem.* **274,** 3557–3564
20. Pettersen, E. F., Goddard, T. D., Huang, C. C., Couch, G. S., Greenblatt, D. M., Meng, E. C., and Ferrin, T. E. (2004) UCSF Chimera—a visualization system for exploratory research and analysis. *J. Comput. Chem.* **25,** 1605–1612
21. Yamaguchi, T., Fujii, T., Abe, Y., Hirai, T., Kang, D., Namba, K., Hamasaki, N., and Mitsuoka, K. (2010) Helical image reconstruction of the outward-open human erythrocyte band 3 membrane domain in tubular crystals. *J. Struct. Biol.* **169,** 406–412
22. Lomize, M. A., Pogozheva, I. D., Joo, H., Mosberg, H. I., and Lomize, A. L. (2012) OPM database and PPM web server: resources for positioning of proteins in membranes. *Nucleic Acids Res.* **40,** D370–D376
23. Benkert, P., Künzli, M., and Schwede, T. (2009) QMEAN server for protein model quality estimation. *Nucleic Acids Res.* **37,** W510–W514
24. Ray, A., Lindahl, E., and Wallner, B. (2012) Improved model quality assessment using ProQ2. *BMC Bioinformatics* **13,** 224
25. Passow, H., Fasold, H., Gärtner, E. M., Legrum, B., Ruffing, W., and Zaki, L. (1980) Anion transport across the red blood cell membrane and the conformation of the protein in band 3. *Ann. N.Y. Acad. Sci.* **341,** 361–383
26. Picollo, A., Malvezzi, M., Houtman, J. C., and Accardi, A. (2009) Basis of substrate binding and conservation of selectivity in the CLC family of channels and transporters. *Nat. Struct. Mol. Biol.* **16,** 1294–1301
27. Lu, F., Li, S., Jiang, Y., Jiang, J., Fan, H., Lu, G., Deng, D., Dang, S., Zhang, X., Wang, J., and Yan, N. (2011) Structure and mechanism of the uracil transporter UraA. *Nature* **472,** 243–246
28. Dutzler, R., Campbell, E. B., Cadene, M., Chait, B. T., and MacKinnon, R. (2002) X-ray structure of a ClC chloride channel at 3.0 Å reveals the molecular basis of anion selectivity. *Nature* **415,** 287–294
29. Krishnamurthy, H., Piscitelli, C. L., and Gouaux, E. (2009) Unlocking the molecular secrets of sodium-coupled transporters. *Nature* **459,** 347–355
30. Faham, S., Watanabe, A., Besserer, G. M., Cascio, D., Specht, A., Hirayama, B. A., Wright, E. M., and Abramson, J. (2008) The crystal structure of a sodium galactose transporter reveals mechanistic insights into Na^+/sugar symport. *Science* **321,** 810–814
31. Weyand, S., Shimamura, T., Yajima, S., Suzuki, S., Mirza, O., Krusong, K., Carpenter, E. P., Rutherford, N. G., Hadden, J. M., O'Reilly, J., Ma, P., Saidijam, M., Patching, S. G., Hope, R. J., Norbertczak, H. T., Roach, P. C., Iwata, S., Henderson, P. J., and Cameron, A. D. (2008) Structure and molecular mechanism of a nucleobase-cation-symport-1 family transporter. *Science* **322,** 709–713
32. Abramson, J., and Wright, E. M. (2009) Structure and function of Na^+-symporters with inverted repeats. *Curr. Opin. Struct. Biol.* **19,** 425–432
33. Zhu, Q., Lee, D. W., and Casey, J. R. (2003) Novel topology in C-terminal region of the human plasma membrane anion exchanger, AE1. *J. Biol. Chem.* **278,** 3112–3120
34. Groves, J. D., and Tanner, M. J. (1999) Structural model for the organization of the transmembrane spans of the human red-cell anion exchanger (band 3; AE1). *Biochem. J.* **344,** 699–711
35. Groves, J. D., and Tanner, M. J. (1999) Topology studies with biosynthetic fragments identify interacting transmembrane regions of the human red-cell anion exchanger (band 3; AE1). *Biochem. J.* **344,** 687–697
36. Tang, X. B., Fujinaga, J., Kopito, R., and Casey, J. R. (1998) Topology of the region surrounding Glu^{681} of human AE1 protein, the erythrocyte anion exchanger. *J. Biol. Chem.* **273,** 22545–22553
37. Fujinaga, J., Tang, X. B., and Casey, J. R. (1999) Topology of the membrane domain of human erythrocyte anion exchange protein, AE1. *J. Biol. Chem.* **274,** 6626–6633
38. Taylor, A. M., Zhu, Q., and Casey, J. R. (2001) Cysteine-directed cross-linking localizes regions of the human erythrocyte anion-exchange protein (AE1) relative to the dimeric interface. *Biochem. J.* **359,** 661–668
39. Popov, M., Tam, L. Y., Li, J., and Reithmeier, R. A. (1997) Mapping the ends of transmembrane segments in a polytopic membrane protein. Scanning *N*-glycosylation mutagenesis of extracytosolic loops in the anion exchanger, band 3. *J. Biol. Chem.* **272,** 18325–18332
40. Kanki, T., Sakaguchi, M., Kitamura, A., Sato, T., Mihara, K., and Hamasaki, N. (2002) The tenth membrane region of band 3 is initially exposed to the luminal side of the endoplasmic reticulum and then integrated into a partially folded band 3 intermediate. *Biochemistry* **41,** 13973–13981
41. Kuma, H., Shinde, A. A., Howren, T. R., and Jennings, M. L. (2002) Topology of the anion exchange protein AE1: the controversial sidedness of lysine 743. *Biochemistry* **41,** 3380–3388
42. Wainwright, S. D., Mawby, W. J., and Tanner, M. J. (1990) The membrane domain of the human erythrocyte anion transport protein. Epitope mapping of a monoclonal antibody defines the location of a cytoplasmic loop near the C-terminus of the protein. *Biochem. J.* **272,** 265–268
43. Hirai, T., Hamasaki, N., Yamaguchi, T., and Ikeda, Y. (2011) Topology models of anion exchanger 1 that incorporate the anti-parallel V-shaped motifs found in the EM structure. *Biochem. Cell Biol.* **89,** 148–156
44. Paw, B. H., Davidson, A. J., Zhou, Y., Li, R., Pratt, S. J., Lee, C., Trede, N. S., Brownlie, A., Donovan, A., Liao, E. C., Ziai, J. M., Drejer, A. H., Guo, W., Kim, C. H., Gwynn, B., Peters, L. L., Chernova, M. N., Alper, S. L., Zapata, A., Wickramasinghe, S. N., Lee, M. J., Lux, S. E., Fritz, A., Postlethwait, J. H., and Zon, L. I. (2003) Cell-specific mitotic defect and dyserythropoiesis associated with erythroid band 3 deficiency. *Nat. Genet.* **34,** 59–64
45. Chu, C., Woods, N., Sawasdee, N., Guizouarn, H., Pellissier, B., Borgese, F., Yenchitsomanus, P. T., Gowrishankar, M., and Cordat, E. (2010) Band 3 Edmonton I, a novel mutant of the anion exchanger 1 causing spherocytosis and distal renal tubular acidosis. *Biochem. J.* **426,** 379–388
46. Guizouarn, H., Borgese, F., Gabillat, N., Harrison, P., Goede, J. S., McMahon, C., Stewart, G. W., and Bruce, L. J. (2011) South-east Asian ovalocytosis and the cryohydrocytosis form of hereditary stomatocytosis show virtually indistinguishable cation permeability defects. *Br. J. Haematol.* **152,** 655–664
47. Zaki, L., Böhm, R., and Merckel, M. (1996) Chemical labelling of arginyl-residues involved in anion transport mediated by human band 3 protein and some aspects of its location in the peptide chain. *Cell. Mol. Biol.* **42,** 1053–1063
48. Böhm, R., and Zaki, L. (1996) Towards the localization of the essential arginine residues in the band 3 protein of human red blood cell membranes. *Biochim. Biophys. Acta* **1280,** 238–242
49. Stewart, A. K., Kedar, P. S., Shmukler, B. E., Vandorpe, D. H., Hsu, A., Glader, B., Rivera, A., Brugnara, C., and Alper, S. L. (2011) Functional characterization and modified rescue of novel AE1 mutation R730C associated with overhydrated cation leak stomatocytosis. *Am. J. Physiol. Cell Physiol.* **300,** C1034–C1046